Endohedral and Exohedral Complexes of Polyhedral Double Four-Membered-Ring (D4R) Units with Atomic and Ionic Impurities

Sung Soo Park, Chuanyun Xiao, and Frank Hagelberg*

Computational Center for Molecular Structures and Interactions, Department of Physics, Atmospheric Sciences, and General Science, Jackson State University, Jackson, Mississippi 39217

Delwar Hossain, Charles U. Pittman, Jr., and Svein Saebo

Department of Chemistry, Mississippi State University, Mississippi State, Mississippi 39762

Received: August 26, 2004; In Final Form: October 6, 2004

Endohedral and exohedral polyhedral cage molecules of the form $(HAO_{3/2})_8$ (A = C, Si, Ge) with double four-membered ring D4R units complexed with the atomic or ionic species (Li^+, Na^+, K^+, F^-, Cl^-, Br^-, He, Ne, Ar) have been investigated at the B3LYP/6-31G(d) and B3LYP/6-311++G(d,p) levels. Geometric, electronic, and energetic properties were obtained. For the endohedral complexes the noble gas atoms (X = He, Ne, and Ar) inside the cage cause the cages to expand, and the extent of the expansion depends on the size of the included atom. Endohedral alkali ions, in contrast, exhibit both attractive and repulsive interactions with the cage atoms. The cage expands when $X = K^+$ and contracts when $X = Li^+$ or Na^+ for A = Si, Ge, and for A = C, the cage expands for all three ions. Encapsulation of the halide ions results in cage expansion throughout. Furthermore, the symmetry of the endohedral complexes when X is a cation depends critically on the relative cation and cage sizes. The binding energies of the endohedral and exohedral complexes document a clear preference for the latter, except for halides, where the endohedral complexes are more stable. The stability of endohedral complexes containing the isoelectronic species $X = Na^+$, Ne, F^- is determined by the charge transfer to the A−O cage bonding sites. The formation of the endohedral complexes is discussed in terms of transition states that connect the exohedral and endohedral minima as well as the activation barriers for insertion of the guest into the cage. Our studies predict that a fluoride anion can penetrate into the $(HAO_{3/2})_8$ cage without destroying it. For $X = Cl^-$, in contrast, the cage ruptures upon insertion of the impurity.

I. Introduction

Octahydridosilsesquioxane, $(HSiO_{3/2})_8$, or polyhedral oligomeric silsesquioxane (POSS) T_8 cage systems and their derivatives have attracted considerable interest.[1] The POSS monomer T_8 cage consists of silicon atoms occupying the vertices of a cube and oxygen atoms bridging each pair of silicon atoms. In the parent octahydridosilsesquioxane a single hydrogen atom is attached to each silicon atom. In general, POSS derivatives exhibit the composition $(RSiO_{3/2})_{2n}$, where R denotes an organic ligand. POSS derivatives incorporated into organic polymers, dendrimers, and zeolites have found substantial attention due to their applications in material science and catalysis.[1] One interesting feature of these cages is that atoms or ions can be encapsulated into them, and several studies, including our own, have focused on this property. Most experimental and theoretical studies[2] reported in the literature have focused on the pure or metal-substituted parent POSS cage with or without encapsulated species. We will comment on endohedral and exohedral complexes, and throughout this article we will use $X@(HAO_{3/2})_8$ to denote the first and $X(HAO_{3/2})_8$ for the second of these structural alternatives.

The structure of the parent T_8-cage molecule $(HSiO_{3/2})_8$ has been characterized by IR and NMR in solution as well as X-ray and neutron diffraction in the solid state and mass spectrometry in the gas phase.[3] Matsuda et al.[4] and Päch et al.[5] studied the double four-membered-ring (D4R) silicate cage with an encapsulated hydrogen atom by ESR spectroscopy. Taylor et al. synthesized an endohedral molecule, octaphenyl octasilsesquioxane fluoride, as a quaternary ammonium salt, confirming its structure by ^1H NMR, ^{29}Si NMR, negative-ion fast atom bombardment (FAB) mass spectrometry, and X-ray diffraction.[6]

The properties of POSS and its derivatives and the reaction path that leads to the incorporation of foreign atomic or ionic species into the POSS cage can be obtained from computational studies. Such studies also may predict novel complexes for future experimental examination. Thus, Mattori et al. reported computational results on the trapping and release transition states (TS) of atomic hydrogen in an octasilsesquioxane host cage.[7] Sodium cations form exohedral complexes with POSS according to ion mobility studies and molecular mechanics (MM) calculations.[8] Encapsulation of Na^+, F^-, or OH^- inside $[(OH)SiO_{3/2}]_8$ has been investigated by local density functional (LDF) techniques.[9] The geometric structures of these composites, as well as the charge redistribution among the host cage and the endohedral ionic species, were predicted. Furthermore, a spherogermante species with D4R units based on germanium is as important as spherosilicate in many technological applications. It is also an interesting object of study as a host cage.[10] Morris et al.[11] prepared for the first time a molecular fluoride-encapsulated octaspherogermante, $F^-@[(OH)GeO_{3/2}]_8$. The structure was confirmed by NMR and X-ray diffraction experiments.[11] The $(HAO_{3/2})_8$ cages (A = C, Si, Ge) are expected to have numerous properties in common since carbon, silicon, and germanium share tetrahedrally coordinated bulk structures. In

10.1021/jp046136r CCC: $27.50
Published on Web 11/24/2004

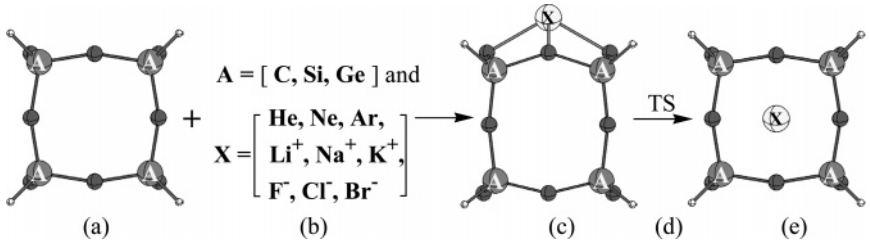

Figure 1. Schematic representation of host cage species with D4R units and impurities: (a) host cage with O_h or T_h symmetries, (b) specification of vertex atoms (A) and impurities (X), (c) exohedral species, and (e) endohedral species are connected by a transition state (d).

fact, $(HGeO_{3/2})_8$ has not been synthesized yet, though analogous systems with other groups replacing the hydrogen are known in inorganic chemistry. For example, fluorine-encapsulated octahydroxylspherogermanate, $F^-@[(OH)GeO_{3/2}]_8$,[11] containing D4R units, has a backbone analogous to that of $(HSiO_{3/2})_8$. Further, an arrangement of cyclic ether compounds[12] is similar to $(HCO_{3/2})_8$, although it has not been synthesized as a cage molecule so far.

Computational results have been reported for the structures and reaction mechanisms of the endohedral complexes $X@(HSiO_{3/2})_8$ ($X = N_2$ and O_2)[13] as well as $H@(HSiO_{3/2})_8$.[7] However, very little information exists about the structures arising from the combination of atomic noble gas atoms, halides, or alkali metal ions with $(HAO_{3/2})_8$ cages. Nothing is known about the formation process of these endohedral and exohedral complexes beyond the pioneering synthetic encapsulation of F^- by Taylor et al.[6] These issues, however, are of relevance both for a systematic understanding of POSS and POSS analogues and for the possible fabrication of both exohedral and endohedral D4R unit complexes.

In this study, we address the question to what extent the geometric, energetic, and electronic properties of $(HAO_{3/2})_8$ can be influenced by addition of atomic and ionic impurities. More specifically, we investigated the exohedral $X(HAO_{3/2})_8$ and endohedral $X@(HAO_{3/2})_8$ [X = He, Ne, Ar, Li^+, Na^+, K^+, F^-, Cl^-, Br^-; A = C, Si, Ge] systems (Figure 1). The most likely direct insertion mechanism is assumed to be the passage of impurities through a square face of the cubic POSS structure. We evaluated the energy barriers involved in the formation of stable endohedral or exohedral structures and assessed the prospects for fabricating endohedral complexes. This work should contribute to understanding the design and control of these molecular systems and to support ongoing endeavors to create new polyhedral sphero-atomic oxide materials with novel properties.

II. Computational Details

All calculations were performed using the Gaussian98[14]and PQS[15] suite of programs. For all species the geometries and the harmonic vibrational frequencies were determined with density functional (DFT) calculations employing the B3LYP[16] potential. It has been demonstrated that this method combined with a basis set of at least a double-ζ plus polarization quality yields reasonable molecular structures and frequencies for many systems.[17c] The vibrational frequencies were calculated for all optimized structures to allow classification of the various structures as minima or transition states; in addition, it allowed corrections of calculated energy differences[17] for differences in zero-point vibrational energies.

Initially, all structures were studied using the 6-31G(d) basis set, and subsequently, refined calculations were carried out employing the 6-311++G(d,p) basis. For the host cage $(HSiO_{3/2})_8$, however, the geometry optimizations and frequency computations were also performed at the B3LYP/6-311++G(2d,p) level to resolve small structural differences between experimentally detected isomers (see section III). For the parent $(HSiO_{3/2})_8$ cage additional calculations using the cc-pVDZ and cc-pVTZ basis sets[18] were carried out for comparison. The agreement of the B3LYP/6-311++G(d,p) results with those obtained at the B3LYP/cc-pVDZ level is typically on the order of 1−2%, which improves to about 0.5% as the B3LYP/cc-pVTZ method is applied.

Application of a method that explicitly includes electron correlation would have been preferable for a study of this nature; however, even the least expensive correlation method (MP2) turned out to be too time-consuming for this study. However, the geometry of the parent POSS cage was optimized at the MP2/6-311G(d,p) level, and the geometry was found to be similar to the geometry obtained at the B3LYP level. The LYP potential does incorporate some correlation effects, and the B3LYP method was chosen as a cost-effective compromise for our studies. The scheme followed in the present calculations is illustrated in Figure 1. The binding energies, BE_{exo} (kcal/mol), of the exohedral clusters were evaluated by taking the energy difference of $X(HAO_{3/2})_8$ (E_{exo}) and the sum of the energies of the isolated components, E_x and E_{pure}. The binding energies for the endohedral complexes, BE_{endo} (kcal/mol), were calculated in an analogous manner. The path between both stable structures and the energy barriers were determined by identifying the transition state (TS; BE_{TS}), separating the exohedral from the endohedral complexes. For each identified transition state we confirmed that it connects the endohedral and the exohedral minimum by careful inspection of the unstable mode. The counterpoise method[19] was used for estimating the size of BSSE of the binding energies, BE_{endo} and BE_{exo} (Supporting Information). These calculations yield a slight modification of the endohedral binding energies without affecting their trends. For the exohedral binding energies, the BSSE has been found to be extremely small.

Adiabatic ionization potentials (IP) were computed for the pure host cages $(HAO_{3/2})_8$ with A = C, Si, Ge as the difference between the total energies of the optimized cations and the optimized neutrals. For the treatment of the cationic cages an unrestricted formalism was used.

III. Results and Discussion

This section is organized the following way: The geometrical features will be discussed first starting with the pure host cages, followed by the endohedral and exohedral complexes, and finally the transition states separating the exohedral and endohedral complexes. In the last section of this part, the energetics, i.e., the binding energies and activation barriers, will be discussed.

Geometrical Features. Host Cages. The geometric parameters of the host cages calculated with the B3LYP method are summarized in Figure 2. Only symmetry unique parameters are

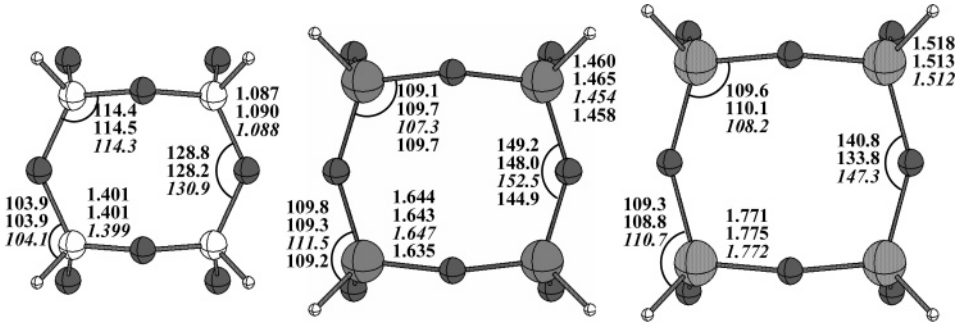

(a) $(HCO_{3/2})_8$; T_h (b) $(HSiO_{3/2})_8$;, O_h or T_h (c) $(HGeO_{3/2})_8$; T_h

Figure 2. Optimized geometries (Å and deg) and molecular point groups of $(HAO_{3/2})_8$ molecules calculated with the B3LYP method, using two different basis sets. The order is (from above) 6-311++G(d,p) and 6-31G(d). Data referring to the structures of the cations are printed in italics; the respective results are obtained on the B3LYP/6-311++G(d,p) level. For $(HSiO_{3/2})_8$, data pertaining to T_h symmetry, obtained at the B3LYP/6-311++G(2d,p) level, are included as the fourth entry in each column.

TABLE 1: Magnitudes of the Lowest Vibrational Frequencies (ω_1), Adiabatic Ionization Potentials (IP), Cage Radii, and Relative Energy (ΔE) between O_h and T_h Isomers at B3LYP/6-311++G(d,p)[a]

	C (T_h)	Si (T_h)	Ge (T_h)
ω_1 (cm^{-1})[b]	218	74[a]	69
IP (eV)	10.15	10.02	9.72
cavity radius (Å)[c]	0.439	0.986	1.129
ΔE (kcal/mol)[d]	13.6	0.7[a]	2.8

[a] At B3LYP/6-311++G(2d,p) optimized structures. [b] Lowest frequency. [c] Cavity radius = [distance between cage center and edge − anionic oxygen radius]. [d] ΔE = total energy (O_h) − total energy (T_h).

shown. Table 1 contains the lowest vibational frequency, the adiabatic ionization potentials (IP), the cavity radii (see footnote c of Table 1) as well as energy differences between the O_h and T_h isomers. It should be noted that the global minimum exhibits T_h symmetry in each case, i.e., for A = C, Si, and Ge. This is consistent with experimental findings which yielded O_h symmetry for $(HSiO_{3/2})_8$ in solution[20] and T_h in the gas phase.[3b] The respective O_h and T_h structures also turned out to be very similar as can be seen in Figure 2. While these two isomers are near-degenerate for the silicate cage, their energies are well separated from each other for the analogous carbonate and germanate cages. From Figure 2, it is also seen that the geometric differences between the host cages and their cations are small.

As expected, the bond lengths r_{A-O} and r_{A-H} increase for the series A = C, Si, Ge, and the host cage sizes relax in the same order. The radii of the host cavities (C, 0.439 Å; Si, 0.986 Å; Ge, 1.129 Å) are sufficient to encapsulate both ionic and atomic species.

The octahydridospherocarbonate $(HCO_{3/2})_8$ and octahydridospherogermanate $(HGeO_{3/2})_8$ cages both have T_h symmetry, and they are 13.6 and 2.8 kcal/mol more stable than their O_h alternatives, respectively. The latter are stationary points with one imaginary (i153) and four imaginary (i75 and triply degenerate i24) frequencies at the B3LYP/6-311++G(d,p) level. Spherogermanate is referred to as a D4R unit in zeolite,[21] and its germanium atoms are tetrahedrally coordinated, just as Si in silicate. Ideally, if O_h symmetry is assumed, the AOA angle should be close to 148°.[21] However, if the symmetry is reduced to T_h (Figure 2), the AOA bond angles are smaller for all three cages.

No experimental data exist for the molecule $(HCO_{3/2})_8$, but geometric parameters observed for methoxymethane (∠COC = 111.7°, r_{C-O} = 1.410 Å)[22] compare well with our results for $(HCO_{3/2})_8$ (∠COC = 112.7°, r_{C-O} = 1.413 Å).[23] The analogous quantities for disiloxane and $(HSiO_{3/2})_8$ are known from experiment and turn out to be very similar. Thus, for disiloxane, the reported geometric parameters are ∠SiOSi = 144.1° and r_{A-O} = 1.634 Å [24], and the respective values for $(HSiO_{3/2})_8$ are ∠SiOSi = 141.7° and r_{Si-O} = 1.649 Å.[23] These findings suggest that our geometry of $(HCO_{3/2})_8$ is realistic.

The isosurface plots of the HOMO and the LUMO are presented in Figure 3 for each of the three host cages. For all cages, the HOMO is preceded by a 3-fold degenerate HOMO−1 and, in reverse order, the LUMO followed by a 3-fold degenerate LUMO+1. In all three cases, the HOMO consists mainly of an oxygen lone pair. The LUMO and the LUMO+1 contain mainly A (C, Si, and Ge) contributions which are antibonding in A−H and A−O.

Endohedral Complexes X@$(HAO_{3/2})_8$. Despite the considerable variations in the sizes of both the host cages and the atomic and ionic endohedral species, stable endohedral geometries were obtained for all complexes investigated in this study. The geometric deformations induced by the encapsulated species were small. Table 2 contains the total energies, point groups, endohedral binding energies, and optimized bond lengths for the endohedral complexes X@$(HAO_{3/2})_8$ with X = Li^+, Na^+, K^+, F^-, Cl^-, Br^-, He, Ne, Ar and A = C, Si, Ge.

Most of the endohedral complexes retain the symmetry of the respective pure host cage, i.e., O_h or T_h. However, this is not observed for Li^+@$(HSiO_{3/2})_8$ or Li^+@$(HGeO_{3/2})_8$. The former turns out to be a stationary point as O_h symmetry is imposed on the system, and likewise, the latter was found to be a stationary point in T_h symmetry conditions. Frequency analysis results in five imaginary frequencies for both these structures (see Supporting Information). Deforming the systems along their triply and doubly degenerate unstable coordinates, we find minima with both D_{2d} and D_{4h} symmetry for Li^+@$(HSiO_{3/2})_8$ and D_{2d} and D_{2h} symmetry for Li^+@$(HGeO_{3/2})_8$, respectively. The coordination of the lithium cation is tetrahedral for the D_{2d} geometry and tetraplanar for the D_{4h} and D_{2h} structures (Figure 4). For both systems the D_{2d} structures are more stable than the D_{4h} and D_{2h} forms by 3.4 and 12.6 kcal/mol for Li^+@$(HSiO_{3/2})_8$ and Li^+@$(HGeO_{3/2})_8$, respectively. In contrast, the endohedral complex Li^+@$(HCO_{3/2})_8$ has a T_h minimum because the cage is too small to permit its oxygen atoms to deform toward the Li^+ ion as in the D_{2d} and D_{4h} cases of Li^+@$(HSiO_{3/2})_8$ and in the D_{2d} and D_{2h} cases of Li^+@$(HGeO_{3/2})_8$. The bond distances between Li and its nearest O atom neighbors for the most stable structures are 2.292 Å [Li^+@$(HCO_{3/2})_8$] (T_h), 2.045 Å [Li^+@$(HSiO_{3/2})_8$] (D_{2d}), and 1.917 Å [Li^+@$(HGeO_{3/2})_8$] (D_{2d}), as seen in Table 2.

The distance r_{X-O} of the host cages (using the convention that "X" denotes the geometric center of the pure cage) shrinks

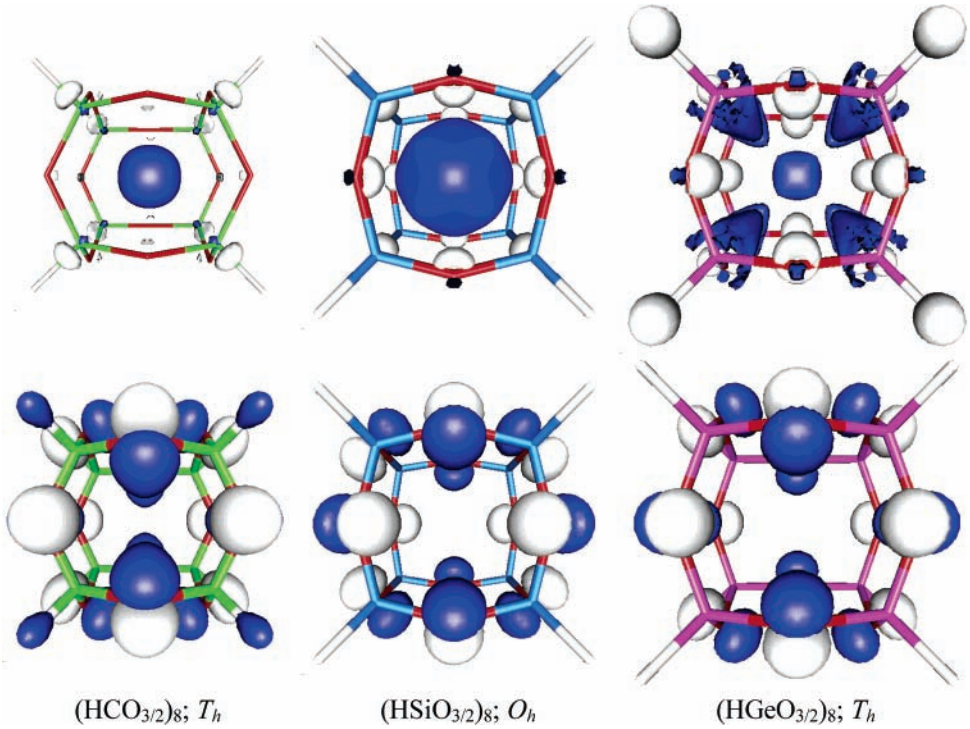

Figure 3. Isosurfaces (dark, positive; light, negative values) for the HOMO and LUMO of the host cages considered in this work (upper row, LUMOs; lower row, HOMOs; isosurface parameter, 0.04 e/Å^3).

TABLE 2: Total Energies (in hartrees), Zero-Point Energies (ZPE), Molecular Point Groups, Lowest Vibrational Frequencies ω_1 (cm^{-1}), Zero-Point Corrected Binding Energies (kcal/mol), and Optimized Bond Lengths (Å) for Endohedral Minima of X@$(HAO_{3/2})_8$ Calculated at the B3LYP/6-311++G(d,p) Level

X	energy	ZPE	sym	ω_1	BE_{endo}	r_{X-A}	r_{X-O}	r_{A-O}	r_{A-H}
				A = C					
pure	−1212.54517	123.4	T_h	218		2.189	2.298	1.401	1.087
Li^+	−1219.78009	120.9	T_h	201	28.9	2.227	2.292	1.414	1.085
Na^+	−1374.50168	120.4	T_h	203	79.2	2.255	2.329	1.424	1.084
K^+	−1811.98387	117.4	O_h	11	196.2	2.325	2.434	1.445	1.082
F^-	−1312.45515	125.4	T_h	33	−11.4	2.220	2.404	1.412	1.091
Cl^-	−1672.53241	119.2	O_h	157	194.4	2.273	2.487	1.456	1.090
Br^-	−3786.31231	115.0	O_h	179	286.9	2.295	2.529	1.478	1.090
He	−1215.41449	125.2	T_h	189	29.5	2.207	2.320	1.407	1.086
Ne	−1341.39188	123.5	T_h	117	71.4	2.240	2.365	1.417	1.085
Ar	−1739.73119	119.5	O_h	116	226.9	2.305	2.458	1.450	1.083
				A = Si					
pure	−3225.16019	87.7	O_h	51		2.746	2.679	1.644	1.460
Li^+	−3232.47633	88.8	D_{2d}	96	−18.5	2.745	2.045	1.651	1.456
Na^+	−3387.22991	87.8	O_h	58	11.3	2.804	2.633	1.655	1.454
K^+	−3824.81416	88.2	O_h	110	67.6	2.821	2.656	1.667	1.454
F^-	−3325.16466	89.2	O_h	80	−71.2	2.693	2.746	1.648	1.472
Cl^-	−3685.41998	88.2	O_h	125	28.0	2.724	2.791	1.671	1.470
Br^-	−5799.27129	87.2	O_h	143	79.0	2.738	2.814	1.683	1.469
He	−3228.05663	89.3	O_h	69	12.3	2.751	2.682	1.647	1.460
Ne	−3354.08419	89.1	O_h	84	24.2	2.757	2.690	1.651	1.461
Ar	−3752.56249	88.6	O_h	125	95.9	2.781	2.725	1.669	1.460
				A = Ge					
pure	−17524.47322	72.1	T_h	69		2.889	2.846	1.771	1.518
Li^+	−17531.85396	74.8	D_{2d}	76	−57.4	2.887	1.917	1.778	1.513
Na^+	−17686.58529	73.0	D_{2d}	59	−14.5	2.958	2.267	1.778	1.512
K^+	−18124.18554	71.8	T_h	55	30.2	3.004	2.833	1.782	1.510
F^-	−17624.48548	73.4	T_h	46	−76.3	2.859	2.962	1.772	1.529
Cl^-	−17984.79965	73.1	O_h	69	−13.3	2.894	3.005	1.790	1.527
Br^-	−20098.68039	72.4	O_h	86	19.5	2.907	3.024	1.800	1.527
He	−17527.37564	73.2	T_h	73	8.1	2.903	2.861	1.772	1.518
Ne	−17653.41233	73.0	T_h	60	14.2	2.924	2.885	1.774	1.517
Ar	−18051.93619	72.7	O_h	53	57.7	2.961	2.933	1.785	1.516

considerably as Li^+ is inserted into $(HSiO_{3/2})_8$ or $(HGeO_{3/2})_8$, while this distance decreases slightly in the case of $(HCO_{3/2})_8$. The Li−A bond lengths, r_{X-A}, connecting the Li^+ ion with the vertices, are 2.227 Å [Li^+@$(HCO_{3/2})_8$], 2.745 Å [Li^+@$(HSiO_{3/2})_8$], and 2.887 Å [Li^+@$(HGeO_{3/2})_8$]. The lithium ion was the smallest endohedral ion considered, and when this ion is inserted into the cage, the original T_h symmetry of the cage is reduced to D_{2d} in order to maximize the electrostatic

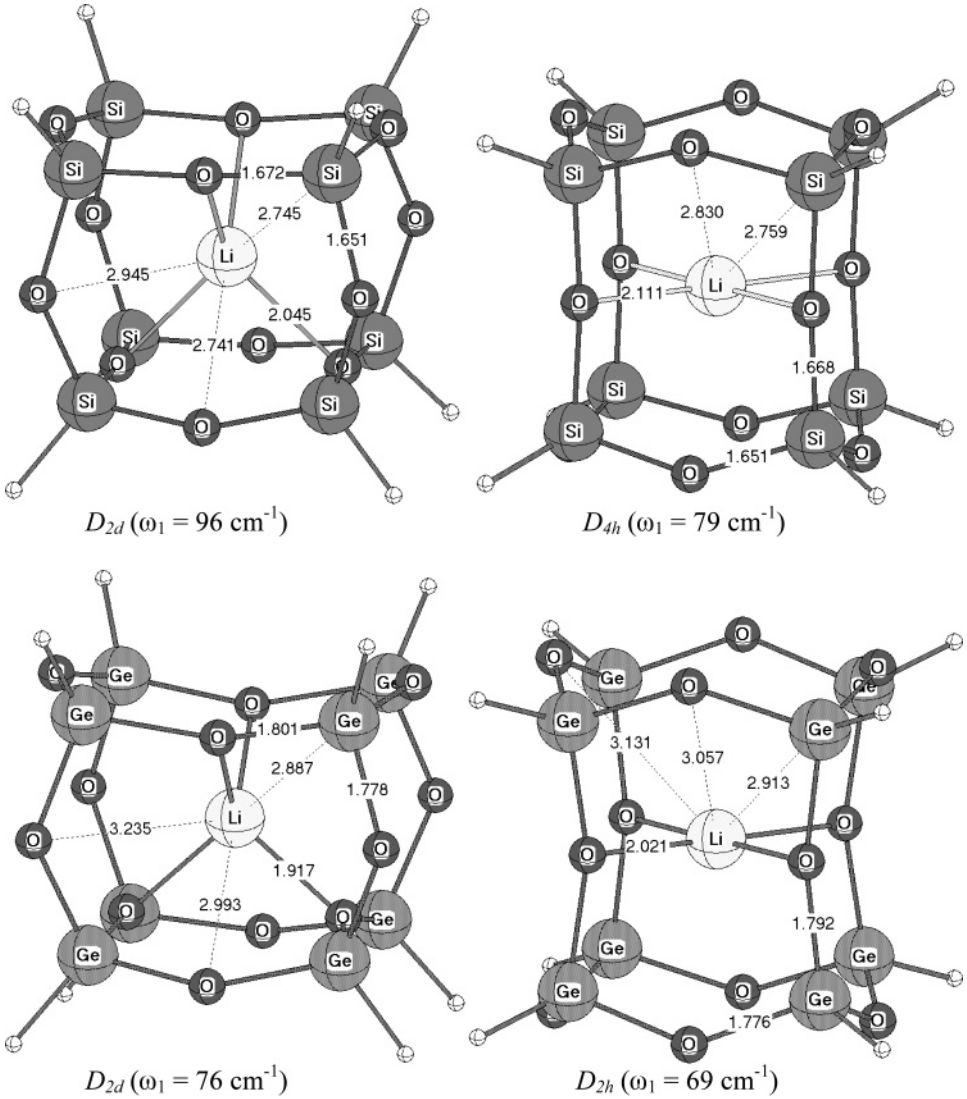

Figure 4. Optimized geometries of $Li^+@(HSiO_{3/2})_8$ and $Li^+@(HGeO_{3/2})_8$ at the B3LYP/6-311++G** level.

interaction between the cation and the cage. This is analogous to the solvation/complexation of alkali ions by crown ethers.[25]

In the endohedral Na^+ systems, the T_h structure of $Na^+@(HGeO_{3/2})_8$ represents a stationary point with two imaginary frequencies. It also distorts to adopt D_{2d} symmetry. In contrast, the $Na^+@(HSiO_{3/2})_8$ and $Na^+@(HCO_{3/2})_8$ minima exhibit O_h and T_h symmetry, respectively. Clearly, the symmetry of the endohedral complexes depends on the relative size of the inserted cation and the size of the cage. For Li^+, the smallest alkali cation, distortion of the cages occurs for the two largest cages (A = Si, Ge) while for Na^+ cage distortion is found only for the largest cage (A = Ge), and no distortion occurred for any of the cages when the largest alkali metal ion, K^+, was inserted. It should be noted that in the cases where no cage distortion was observed D_{2d} structures were not stationary points on the potential surfaces.

The A−O bond distances of all the endohedral cationic metal complexes are longer than the respective distances in the pure host cages and lengthen as the size of the endohedral cations (X = Li^+, Na^+, K^+) and the vertex atoms (A = C, Si, Ge) increase. Natural charge analysis,[26] as shown in Table 3, reveals that the cationic species induce not only the transfer of electron density from the A−H bonds to the A−O bonds of the $(HAO_{3/2})_8$ host cages but also accept electron density from the host cages (see Table 3 for numerical details). The amount of charge transfer decreases in the order $Li^+ > Na^+ > K^+$. The endohedral $K^+@(HAO_{3/2})_8$ complexes have the shortest A−H bond lengths (C, 1.082 Å; Si, 1.454 Å; Ge, 1.510 Å), while the $Li^+@(HAO_{3/2})_8$ complexes have the longest (C, 1.085 Å; Si, 1.456 Å; Ge, 1.513 Å).

The endohedral halide (X = F^-, Cl^-, Br^-) complexes all retain the high symmetry of the parent cage (O_h or T_h). All endohedral halide complexes exhibit O_h symmetry, with the exception of $F^-@(HAO_{3/2})_8$ with A = C, Ge which resulted as a T_h structure. Geometries with lower symmetries (e.g. D_{2d}) were also considered, but these structures revert to the more symmetrical T_h or O_h structures.

In contrast to the alkali metal ions, the halides transfer electron density to the host cages. Electron donation occurs from endohedral halides to both the A−O bonds and the hydrogen sites (with a slight irregularity for X = F and A = Si, Ge). Both the A−O and A−H distances elongate as a consequence of halide implantation. This observation is in accordance with a computation of the $(HSiO_{3/2})_8$ anion at the B3LYP/6-311++G(d,p) level. For the anion as compared with the neutral we find elongation of the Si−O and the Si − H bonds by 0.003 and 0.01 Å, respectively. These values are in close proximity of the respective bond length extensions found upon encapsulation of F^- into $(HSiO_{3/2})_8$ (see Table 2). The largest elongation of A−O and A−H distances was obtained for the smallest cage

TABLE 3: Natural Charge Analysis of Endohedral Minima at the B3LYP/6-31G(d) Level

	A = C			A = Si			A = Ge		
X	Q_X[a]	ΣQ_{AO}[b]	ΣQ_H	Q_X[a]	ΣQ_{AO}[b]	ΣQ_H	Q_X[a]	ΣQ_{AO}[b]	ΣQ_H
pure		−1.89	1.89		1.92	−1.92		1.50	−1.50
Li^+	0.85	−2.13	2.28	0.86	1.71	−1.57	0.85	1.26	−1.11
Na^+	0.88	−2.21	2.33	0.83	1.74	−1.57	0.85	1.25	−1.10
K^+	0.95	−2.42	2.47	0.91	1.60	−1.52	0.88	1.17	−1.06
F^-	−0.68	−2.03	1.71	−0.71	1.95	−2.24	−0.69	1.53	−1.85
Cl^-	−0.26	−2.58	1.84	−0.58	1.69	−2.11	−0.58	1.31	−1.74
Br^-	0.08	−2.94	1.86	−0.44	1.52	−2.08	−0.44	1.13	−1.69
He	0.05	−2.00	1.95	0.04	1.86	−1.90	0.04	1.45	−1.49
Ne	0.09	−2.10	2.01	0.07	1.82	−1.89	0.07	1.41	−1.48
Ar	0.27	−2.43	2.16	0.16	1.66	−1.82	0.15	1.25	−1.40

[a] Q_X = charge on impurity X. The symbols Q_A, Q_H, and Q_O are defined analogously. [b] $\Sigma Q_{AO} = \Sigma Q_A + \Sigma Q_O$.

TABLE 4: Total Energies (in hartrees), Lowest Frequencies ω_1 (cm^{-1}), Molecular Point Groups, Binding Energies (kcal/mol), Optimized Bond Lengths (Å), and Natural Charges on Metal Atoms (Q_X) for Exohedral Minima of Cationic Metal Complexes Calculated at the B3LYP/6-311++G(d,p) Level

A	X	energy	ω_1	sym	BE_{exo}	r_{X-A}	r_{X-O} (r'_{X-O})	r_1 (r'_1)	r_2	r_3	r_4 (r'_4)	Q_X[a]
C	Li^+	−1219.90380	129	C_{2v}	−45.2	2.743	2.661(1.921)	1.454 (1.414)	1.362	1.420	1.392 (1.392)	0.94
	Na^+	−1374.68020	61	C_{2v}	−29.4	3.118	3.025 (2.320)	1.440 (1.413)	1.369	1.417	1.393 (1.393)	0.97
	K^+	−1812.33629	39	C_{2v}	−18.7	3.517	3.424 (2.735)	1.431 (1.411)	1.374	1.415	1.394 (1.394)	0.98
Si	Li^+	−3232.52175	78	C_{4v}	−46.7	2.730	2.087	1.678	1.611	1.663	1.640	0.92
	Na^+	−3387.29599	75	C_{4v}	−29.6	3.125	2.501	1.672	1.614	1.660	1.640	0.96
	K^+	−3824.95055	69	C_{4v}	−18.0	3.553	2.955	1.666	1.617	1.658	1.641	0.98
Ge	Li^+	−17531.85935	35	C_{2v}	−62.1	2.821	2.221(1.968)	1.812 (1.797)	1.737	1.785	1.765 (1.767)	0.88
	Na^+	−17686.62766	36	C_{4v}	−41.4	3.173	2.442	1.802	1.729	1.777	1.766	0.95
	K^+	−18124.27746	18	C_{2v}	−26.7	3.647	3.249 (2.710)	1.805 (1.787)	1.742	1.782	1.767 (1.768)	0.98

[a] At the B3LYP/6-31G(d) level.

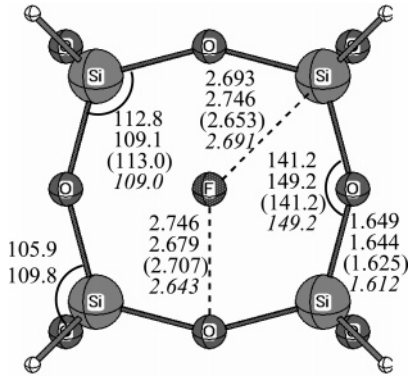

Figure 5. Optimized geometry of $F^-@(HSiO_{3/2})_8$ with O_h symmetry at the B3LYP/6-311++G(d,p) level. For comparison, the structural data of the pure $(HSiO_{3/2})_8$ cage are included in the second entry of each column. The experimental values of $F^-@[(Ph)SiO_{3/2}]_8$ and $[(Ph)SiO_{3/2}]_8$ are printed in parentheses and in italics, respectively.

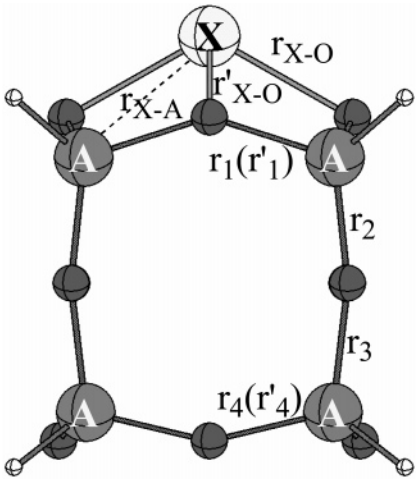

Figure 6. Schematic geometry for the $X^+(HSiO_{3/2})_8$ complex with X = alkali metal species. The primed symbols refer to C_{2v} and the unprimed to C_{4v} symmetry (see text).

$(HCO_{3/2})_8$. This may be attributed to the smaller initial cage and the tendency of the $(HCO_{3/2})_8$ cage to accommodate the electronic charge donated by the halogen species. The amount of electron donation from the anionic halide to the host cage increases in the order $F^- < Cl^- < Br^-$.

$F^-@(HSiO_{3/2})_8$ has the longest Si−H (1.472 Å) and the shortest X−Si bond length (2.693 Å) among the octahydridosilsesquenoxane derivatives discussed here. The Si−O and Si−H bond lengths are longer and the X−Si bond lengths are shorter in the halide endohedral complexes compared to the alkali ion counterparts with X = Na^+, K^+ (Table 2). The experimental distances between the silicon atoms and the cage center in $F^-@[(Ph)SiO_{3/2}]_8$ and $[(Ph)SiO_{3/2}]_8$[6] (Figure 5) are a little shorter in the endohedral F^- species (2.653 Å) than in the isolated host cage (2.691 Å), and the experimental X−O distance is longer in the endohedral species (2.707 Å) than in the isolated host cage (2.643 Å). Furthermore, the Si−O bonds (1.625 Å) are longer and ∠SiOSi angles (141.2°) are smaller in $F^-@[(Ph)SiO_{3/2}]_8$ than in $[(Ph)SiO_{3/2}]_8$ (Si−O = 1.612 Å, ∠SiOSi = 149.2°). These experimental trends are consistent with our calculated results.

For endohedral complexes $X@(HAO_{3/2})_8$ where X is a neutral noble gas atom (He, Ne, or Ar), the geometric changes are almost negligible for He and Ne but significantly larger when X = Ar. The smallest cage, $(HCO_{3/2})_8$, exhibits the largest expansion upon insertion of a noble gas species, and naturally X = Ar gives rise to the strongest effect. Details can be found in Table 2.

Exohedral Complexes $X(HAO_{3/2})_8$. Table 4 summarizes selected geometric parameters and binding energies for the optimized exohedral D4R complexes involving alkali metal cations, $X(HAO_{3/2})_8$ (X = Li^+, Na^+, K^+; A = C, Si, Ge). The bond designations used in Table 4 are illustrated in Figure 6. In all of these complexes, the alkali metal cation is attached to

TABLE 5: Total Energies (in hartrees), Zero-Point Corrected Binding Energies (BE_{TS},[a] kcal/mol), and the Single Imaginary Frequencies ω_I for Transition Structures of $(HAO_{3/2})_8$ (A = C, Si, Ge) Calculated at the B3LYP/6-311++G(d,p) Level

	A = C				A = Si				A = Ge			
X	E_{TS}	sym	BE_{TS}	ω_I	E_{TS}	sym	BE_{TS}	ω_I	E_{TS}	sym	BE_{TS}	ω_I
Li^+	−1219.75753	C_{2v}	43.5	*i*356	−3232.46544	C_{4v}	−11.6	*i*113	−17531.82697	C_s	−41.3	*i*171
Na^+	broken				−3387.12507	C_{4v}	77.3	*I*287	−17686.52321	C_s	24.4	*i*223
K^+	broken				−3824.56875	C_{4v}	218.6	*i*298	−18124.02509	C_s	130.4	*i*230
F^-	broken				−3325.06095	C_s	−7.2	*i*257	n/a			
Cl^-	broken				broken				n/a			
Br^-	broken				broken				n/a			
He	−1215.30454	C_{2v}	98.2	*i*682	−3227.99401	C_{4v}	52.7	*i*509	−17527.33321	C_{2v}	35.7	*i*373
Ne	broken				−3353.94742	C_{4v}	109.3	*i*323	−17653.32281	C_{2v}	70.4	*i*243
Ar	broken				−3752.30757	C_{4v}	252.6	*i*283	−18051.74862	C_s	173.9	*i*230

[a] $BE_{TS} = E_{TS} - [X + (HAO_{3/2})_8]$.

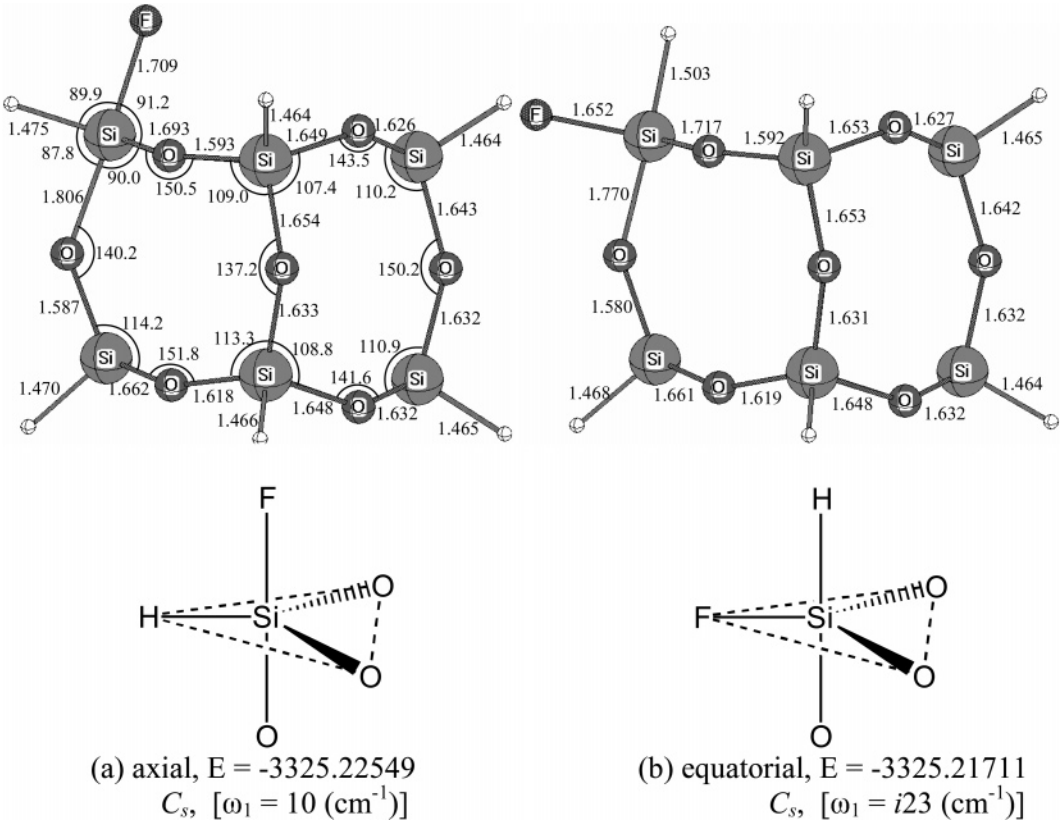

Figure 7. Optimized geometries of two isomers of exohedral $F^-(HSiO_{3/2})_8$ with C_s symmetry at the B3LYP/6-311+G(2d,p) level.

a face of the cage. Clearly, an exohedral impurity will destroy the high symmetry of the host cage system; specifically, all exohedral complexes have C_{2v} or C_{4v} symmetry. The X−O bond lengths for $X(HAO_{3/2})_8$ with X = Li^+, Na^+ and A = Si, Ge are similar to the distances in the respective endohedral systems; the same holds for the X−A bond lengths when X = Li^+ and A = Si, Ge. In both types of complexes the Li^+ ion interacts with four oxygen atoms. Both the exohedral and the endohedral addition of a Li^+ ion to the pure D4R cages are exothermic processes (see below). Only minor changes, in the range of ±0.04 Å, occur in the A−O bond lengths (r_1 to r_4) in the face adjacent to the alkali ion and in the opposite face (see Figure 6 and Table 4).

Halide complexes of the form $X^-(HAO_{3/2})_8$ (X = F, Cl, Br) were studied for A = Si. Figure 7a,b shows the geometric parameters for exohedral $F^-(HSiO_{3/2})_8$, resulting from initial optimization at the B3LYP/6-31G(d) and B3LYP/6-311++G(d,p) levels and subsequent B3LYP/6-311+G(2d,p) computation. The $HSiO_3F^-$ subunit adopts a regular trigonal-bipyramidal structure. The main geometric difference between the isomers shown in Figure 7a,b is that F^- occupies an axial position within

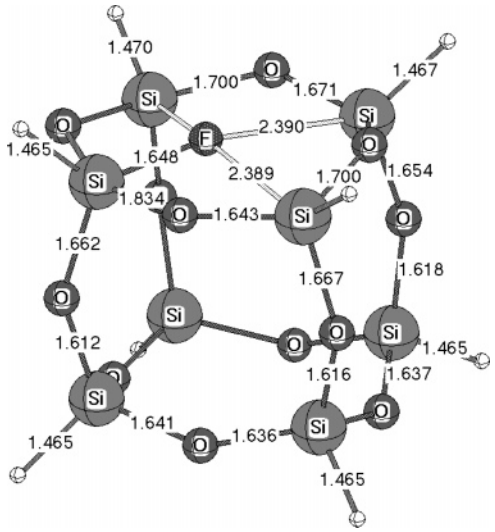

Figure 8. Transition structure connecting the exohedral and the endoheral minimum of $F^-(HSiO_{3/2})_8$ with C_s symmetry at the B3LYP/6-311+G(2d,p) level.

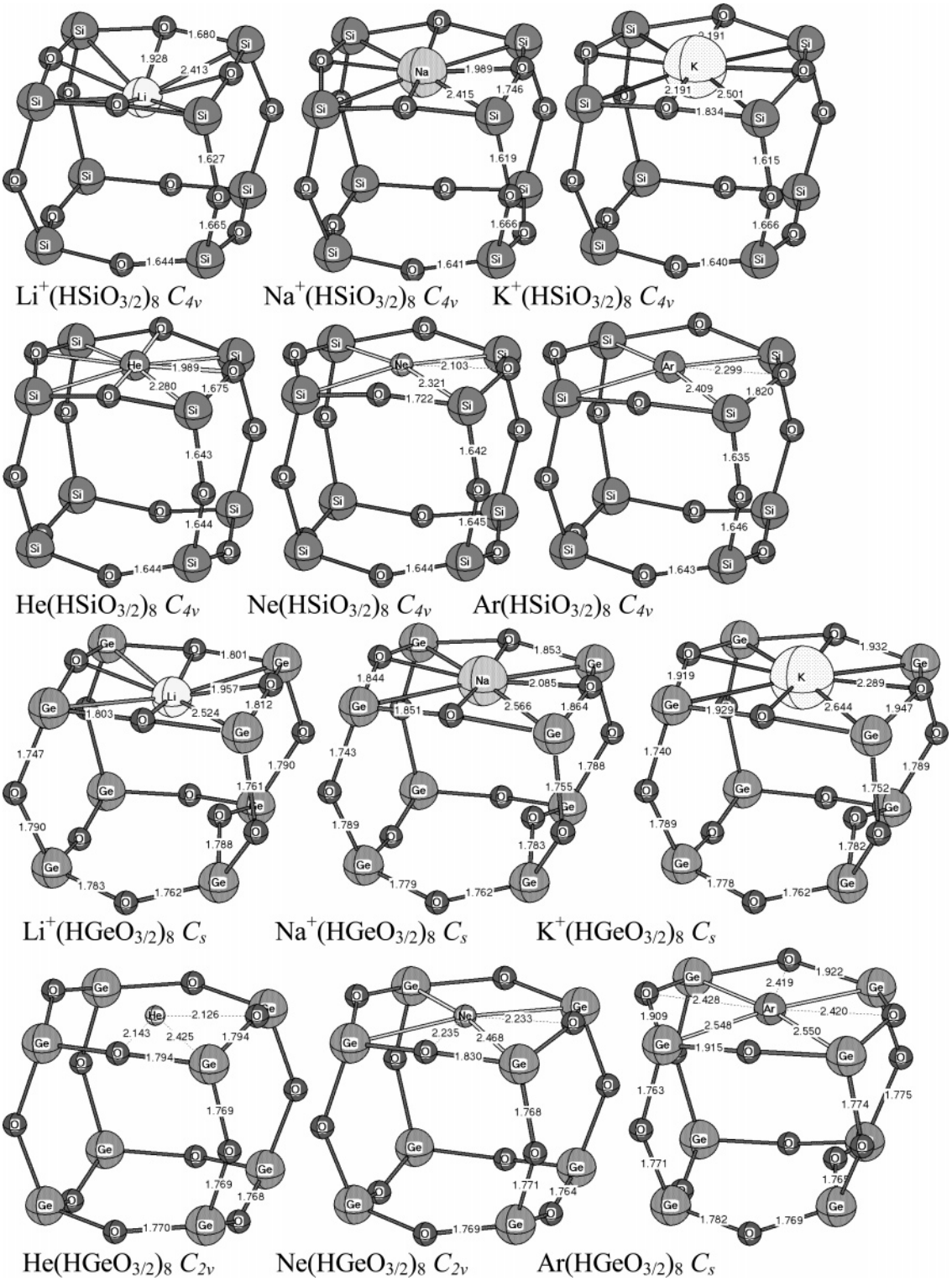

Figure 9. Transition structures for atomic rare gas species (He, Ne, Ar) and alkali cations (Li^+, Na^+, K^+) in $(HAO_{3/2})_8$ cages with A = Si, Ge, at the B3LYP/6-311++G(d,p) level.

this bipyramid in Figure 7a and an equatorial position in Figure 7b. The location of F^- is in sharp contrast to the face location adopted by alkali metal ions in the exohedral complexes discussed above. The axial fluoride (Figure 7a) exhibits a longer Si−F distance (1.709 Å) than the equatorial fluoride (1.652 Å), and the axial Si−F bond length is significantly longer than the Si−F bond found in tetracoordinated SiF_4 (experimental, 1.56 Å; theoretical, 1.57 Å) and in axial pentacoordinated silyl fluoride (1.67 Å).[26] However, this 1.709 Å bond length is shorter than those reported for pentacoordinated silicon in the SiO_4F^- (1.74 Å) subunit of zeolite.[28] As expected, the Si−O and Si−H bonds of the pentacoordinated silicon atoms that are connected to the exohedral F^- ions are longer than the corresponding bonds in the pure $(HSiO_{3/2})_8$ cage that contains tetracoordinated Si.

No exohedral isomers are included for the noble gas complexes. The respective structures were found to involve large distances on the order of 5−6 Å between the host face and the

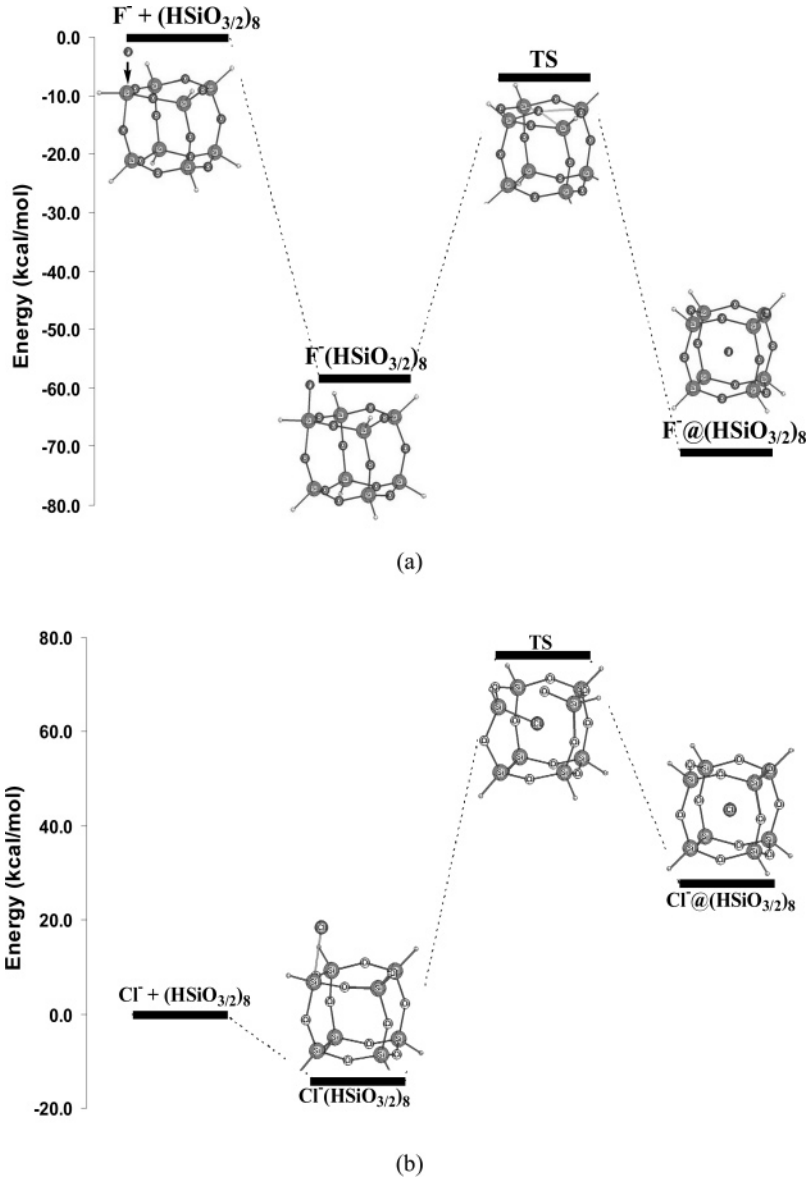

Figure 10. Energy barrier for encapsulation of a fluoride (a) and a chloride (b) anion inside the $(HSiO_{3/2})_8$ cage.

TABLE 6: Binding Energies for Formation of Endohedral (BE_{endo}) and Exohedral (BE_{exo}) Complexes and Relative Energies (E_{rel}[a]) for $(HAO_{3/2})_8$ (A = C, Si, Ge) Calculated at the B3LYP/6-311++G(d,p) Level

	C			Si			Ge		
X	BE_{endo}	BE_{exo}	E_{rel}	BE_{endo}	BE_{exo}	E_{rel}	BE_{endo}	BE_{exo}	E_{rel}
Li^+	28.9	−45.2	74.1	−18.5	−46.7	28.2	−57.4	−62.1	4.7
Na^+	79.2	−29.4	108.6	11.3	−29.6	40.9	−14.5	−41.4	26.9
K^+	196.2	−18.7	214.9	67.6	−18.0	85.6	30.2	−26.7	56.9
F^-	−11.4			−71.2	−58.4	−12.8	−76.3		
Cl^-	194.4			28.0	−14.2	42.2	−13.3		
Br^-	286.9			79.0	−9.5	88.5	19.5		
He	29.5		29.5	12.3		12.3	8.1		8.1
Ne	71.4		71.4	24.2		24.2	14.2		14.2
Ar	226.9		226.9	95.9		95.9	57.7		57.7

[a] $E_{rel} = BE_{endo} - BE_{exo}$. All energies are in kcal/mol.

noble gas atom. Thus, they were hardly distinguishable from the separated species. These very weakly bonded complexes could be artifacts caused by basis set superposition errors.

Transition States. The transition states that separate the endohedral and exohedral structures are summarized in Table 5. These transition states are encountered as the guest species is forced through the face of cage from outside to inside. In this subsection, the identified transition states are characterized in terms of geometric properties.

The transition states for halide insertion will be considered first. Transition states were obtained for F^- and Cl^-. The structure of the $F^-(HSiO_{3/2})_8$ transition state complex is shown in Figures 8 and 10a. The fluoride anion is located on a face of the cage.

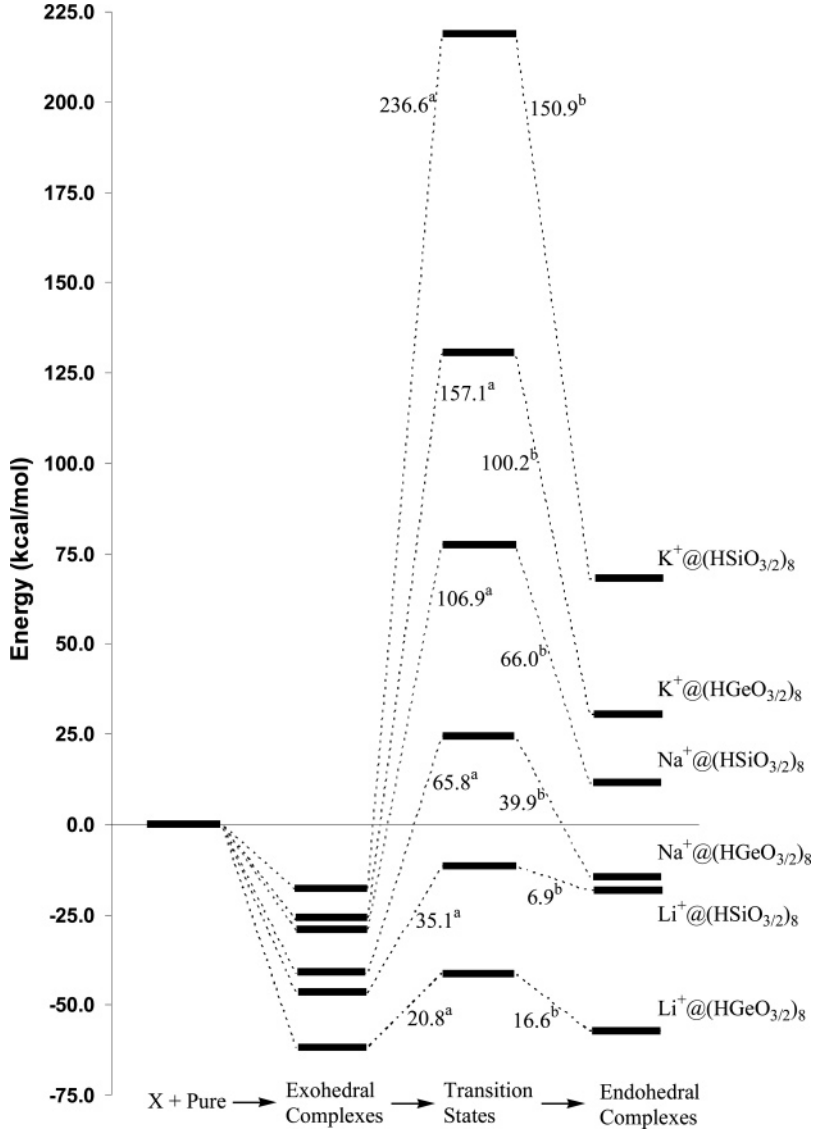

Figure 11. Endothermic and exothermic reaction paths connecting exohedral and endohedral minima as well as transition structures for encapsulation of an alkali cation inside $(HSiO_{3/2})_8$ and $(HGeO_{3/2})_8$. [a]Trapping energies; [b]detrapping energies, both in kcal/mol.

The transition state structures for introducing alkali metal cations and atomic noble gas guests resemble those found for F^-. In each case, the guest species occupies a position at or close to the center of a host face (see Figure 9). In the case of A = C transition states were only found for He and Li^+, probably due to the small face size of this cage. The transition state structures connecting the exohedral and endohedral $X(HSiO_{3/2})_8$ and $X(HGeO_{3/2})_8$ complexes differ somewhat more from each other than the corresponding endohedral geometries do. For example, transition states for introducing alkali metal cations into the $(HSiO_{3/2})_8$ cage have C_{4v} symmetry while the Ge-based transition state adopts C_s symmetry. Structural details can be found in found in Figure 9.

Energetics. We will first discuss the binding energies for formation of the endohedral and exohedral complexes and then discuss the barriers for the insertion processes. Table 6 summarizes the ZPE-corrected endohedral (BE_{endo}) and exohedral (BE_{exo}) binding energies for the species $X@(HAO_{3/2})_8$ and $X(HAO_{3/2})_8$, respectively. These binding energies were calculated as the energy difference between a complex and the sum of the energies of X and the isolated host cage. A negative BE thus indicates that the complex is favored compared to the separated species; i.e., its formation is an exothermic process. All exohedral complexes listed in Table 6 are preferred over the separated species. In contrast, the formation of most of the endohedral complexes was found to be endothermic, excepting the systems $F^-@(HAO_{3/2})_8$ (A = C, Si, and Ge), $Cl^-@(HGeO_{3/2})_8$, $Li^+@(HSiO_{3/2})_8$, and $X@(HGeO_{3/2})_8$ (X = Li^+, Na^+) which were all significantly exothermic (see Table 6 for details). However, there is a substantial difference in binding energies for the systems $Li^+@(HGeO_{3/2})_8$ and $Li^+@(HSiO_{3/2})_8$ (−57.5 and −18.5 kcal/mol, respectively).

As is seen from the values of BE_{endo} in Table 6, the bonding between the encapsulated impurity X and the cage strengthens as the atomic number of X decreases within a group of the periodic table which should simply be a manifestation of the size of the guest species. The impurities F^-, Ne, and Na^+ are isoelectronic. Furthermore, F^- and Na^+ as well as He and Li^+ have approximately equal radii.[29] However, the binding energies of these complexes differ significantly. Thus, the size is of the guest species is only one of the factors that impact the endohedral binding energies. The large differences between the natural charges of guests that are similar in size, as indicated in Table 3, suggest that charge transfer from the impurity to the host cage determines BE_{endo} in the absence of size effects.

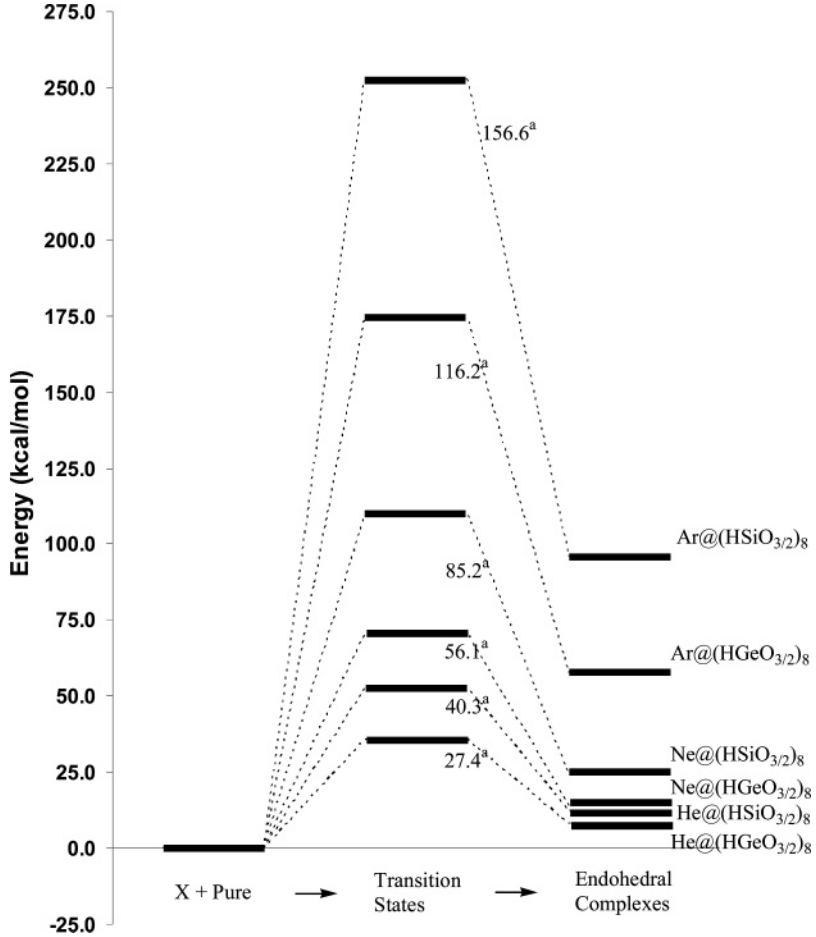

Figure 12. Energy barriers for encapsulation of atomic noble gas species inside $(HSiO_{3/2})_8$ and $(HGeO_{3/2})_8$. [a]Detrapping energies in kcal/mol.

It is interesting to compare the energetic properties of $X@(HAO_{3/2})_8$ with those of the hydrocabon analogues $X@C_{20}H_{20}$.[30] The endohedral binding energies of $X@(HSiO_{3/2})_8$ (X = He, 12.3; Ne, 24.2; Ar, 95.9 kcal/mol) are lower (i.e., the complexes are more stable) than those of $X@C_{20}H_{20}$ (X = He, 37.9; Ne, 102.9; Ar, 320.2 kcal/mol). Furthermore, Li^+ and Na^+ give rise to considerably more stable endohedral composites when enclosed in $(HSiO_{3/2})_8$ (X = Li^+, −18.5; Na^+, 11.3) or in $(HGeO_{3/2})_8$ (X = Li^+, −57.4; Na^+, −14.5) than in $C_{20}H_{20}$ (Li^+, −12.7, Na^+, 55.3 kcal/mol).[30] The same hierarchy of stabilities as established in this work for $X@(HAO_{3/2})_8$ (X = Li^+, Na^+, K^+; A = C, Si, K) was found by Sun et al. in computations on fullerene C_{32} as the host for Li^+ ($Li^+@C_{32}$: −53.1 kcal/mol), Na^+ ($Na^+@C_{32}$: −26.9 kcal/mol), and K^+ ($K^+@C_{32}$: 13.7 kcal/mol), using the GGA DFT procedure.[31] Consistently, the Li^+ incorporating system emerges as most stable, while the K^+ containing unit is of lowest stability.

The exohedral binding energies (BE_{exo}) show a similar charge and size dependence as the endohedral binding energies (BE_{endo}, Table 2). Adsorption of the small Li^+ ion turns out to be the most exothermic process for all three $(HAO_{3/2})_8$ cages, followed by Na^+ and K^+. The energy differences between the exohedral and endohedral structures (the "relative energy", E_{rel}, listed in Table 6) demonstrate that the exohedral species are usually energetically more favorable than the endohedral alternatives. Among the alkali ion-containing complexes, E_{rel} is smallest for Li^+ encapsulated in $(HGeO_{3/2})_8$. Its E_{rel} is only 4.7 kcal/mol, which may be close to the uncertainty of the calculated energy differences in this study.

The smallest noble gas atom, He, embedded in the largest cage, $(HGeO_{3/2})_8$, results in the lowest endohedral binding energy (BE_{endo} = 8.1 kcal/mol, see Table 2). The highest value (226.9 kcal/mol) of BE_{endo} within the noble gas series is given by X = Ar in the $(HCO_{3/2})_8$ cage.

Figures 11 and 12 show schematic energy profiles for formation of the endohedral complex from the corresponding exohedral one for $X(HAO_{3/2})_8$ (A = Si, Ge). X represents an alkali ion in Figure 11 and a noble gas atom in Figure 12. These figures demonstrate that the insertion barriers vary considerably, dependent on the nature of the guest species. The activation barriers between the endohedral and the exohedral minima correlate with the bond stretching that is induced in the face traversed by the guest. Notably, the insertion of Li^+ into $(HAO_{3/2})_8$ (A = Si, Ge) leads through transition states whose energies are lower than the sum of the separated cage and guest energies. This indicates that exothermic entrapping processes occur. This situation is exceptional within the systems studied herein.

The activation barrier for the insertion of F^- ion into the cage is 51.2 kcal/mol. To remove F^- from within the cage the barrier is 64.0 kcal/mol. These results are of interest in the context of a conjecture made by Taylor et al.[6] concerning the $F^-(HSiO_{3/2})_8$ complex: "the fluoride ion must be acting as a template for formation of the cage and once inside it, it can only escape when the cage is broken down." This statement is based on the observation that refluxing the $F^-@[(Ph)SiO_{3/2}]_8$ cluster in various solvents does not lead to the loss of the fluoride ion.[6] Our computation, however, suggests that, in principle, traversal of the F^- impurity through a face of the $(HSiO_{3/2})_8$ host could occur without destruction of the cage. To implant or remove Cl^- or Br^- ion, however, requires breaking the $(HSiO_{3/2})_8$ cage. This feature was confirmed by a computation of the $Cl^-(HSiO_{3/2})_8$

transition state. In this structure, one Si−O bond of the cage is ruptured (see Figure 10b) as the distance between Si and O is elongated to 3.02 Å, and a bond between the Cl^- ion and one Si atom is established with a bonding distance of 2.08 Å. This ruptured transition state is higher in energy than the O_h minimum $Cl^-@(HSiO_{3/2})_8$ by 49.8 kcal/mol.

IV. Conclusions

The D4R cage geometries for $(HAO_{3/2})_8$ (A = C, Si, Ge) all exhibit T_h symmetry, although for A = Si, a less stable minimum with O_h symmetry was also found. The cavities of these cages are sufficiently large to accommodate atomic and ionic guests.

The endohedral complexes, $X@(HAO_{3/2})_8$ (X = Li^+, Na^+, K^+, F^-, Cl^-, Br^-, He, Ne, Ar, where A = C, Si, Ge), were found to have either T_h or O_h symmetry with exception of the three systems $Li^+@(HSiO_{3/2})_8$, $Li^+@(HGeO_{3/2})_8$, and $Na^+@(HGeO_{3/2})_8$, which favor D_{2d} symmetry. Encapsulated noble gas atoms (He, Ne, Ar) expand the cage roughly in proportion to their radii, elongating the A−O bond lengths of the host cages. These calculations predict markedly different features for encapsulated halogen anions than for their isoelectronic nobel gas and alkali metal cations. Thus, for the isoelectronic series F^-, Ne, and Na^+, the Si−O bond lengths increase, while the Si−H bond lengths change in the reverse order. This behavior is understood as the result of charge redistribution between the Si−O and the Si−H bonds of the host cage, as induced by the presence of the guest species.

We identified several guest/host combinations for which guest inclusion is energetically favorable. For A = C, only one such case was obtained, namely X = F, two for A = Si (X = F, Li) and four for A = Ge (X = F, Cl, Li, Na). Charge polarization between the host and the guest turned out to be the principal cause for the stability of these complexes. All endohedral complexes enclosing alkali cations have higher energy than their exohedral counterparts, as suggested by ion mobility studies on various silsesquioxanes cationized by addition of Na^+.[8] The endohedral complexes $F^-@(HAO_{3/2})_8$, where A = Si, Ge, are preferred over the exohedral alternatives, in accord with experiment.[6] Nevertheless, we predict the existence of $F^-(HSiO_{3/2})_8$, with F^- occupying an axial position in a trigonal-bipyramidal subcomplex.

An analysis of the transition states connecting the endohedral and exohedral complexes leads to the prediction that the F^- ionic impurity, in contrast to Cl^- and Br^- ion, might be directly inserted into the $(HSiO_{3/2})_8$ cage without destroying it. Similar transition state structures were identified for the $(HSiO_{3/2})_8$ and $(HGeO_{3/2})_8$ hosts in combination with the alkali cation and noble gas atom guests. The corresponding activation energy barriers were found to depend sensitively on the amount of bond length expansion required for the guest to traverse the face of the cage.

On the basis of our work, we hope that novel host cages composed of D4R units may be synthesized in conjunction with endohedral as well as exohedral alkali metal ion or halide guests.

Acknowledgment. This work is supported by the National Science Foundation through Grants HRD-9805465, NSFESP-0132618, and DMR-0304036, by the National Institute of Health through Grant S06-GM008047, by the Air Force Office of Scientific Research, Grant F49620-02-1-026-0, and by the Army High Performance Computing Research Center under the auspices of Department of the Army, Army Research Laboratory, under Cooperative Agreement DAAD 19-01-2-0014.

Supporting Information Available: Table of point groups, number of imaginary frequencies, and binding energies of $(HAO_{3/2})_8$ with metal cationic impurities; table of diagonal parameters of pure cages; and table of counterpoise corrected binding energies. This material is available free of charge via the Internet at http://pubs.acs.org.

References and Notes

(1) (a) Brown, J. F., Jr.; Vogt, L. H., Jr. *J. Am. Chem. Soc.* **1965**, *87*, 4313−4317. (b) Feher, F. J.; Wyndham, K. D. *Chem. Commun.* **1998**, 323. (c) Maxim, N.; Abbenhuis, H. C. L.; Stobbelaar, P. J.; Mojet, B. L.; van Santen, R. A. *Phys. Chem. Chem. Phys.* **1999**, *18*, 4473. (d) Maxim, N.; Magusin, P. C. M. M.; Kooyman, P. J.; van Wolput, J. H. M. C.; van Santen, R. A.; Abbenhuis, H. C. L. *Chem. Mater.* **2001**, *13*, 2958. (e) Wada, K.; Yamada, K.; Kondo, T.; Mitsudo, T. *Chem. Lett.* **2001**, 12. (f) Dance, B. *Semiconduct. Int.* **2001**, *24*, 46. (g) Lamm, M. H.; Chen, T.; Glotzer, S. C. *Nano Lett.* **2003**, *3*, 989. (h) Zheng, L.; Waddon, A. J.; Farris, R. J.; Coughlin, E. B. *Macromolecules* **2002**, *35*, 2375. (i) Li, G.-Z.; Wang, L.; Ni, H.; Pittman, C. U., Jr. *J. Inorg. Organomet. Polym.* **2001**, *11*, 123. (j) Li, G.-Z.; Wang, Li.; Toghiani, H.; Pittman, C. U., Jr.; Daulton, T. L. *Polymer* **2002**, *43*, 4167. (k) Li, G.-Z.; Wang, L.; Toghiani, H.; Pittman, C. U., Jr.; Daulton, T. L.; Koyama, K. *Macromolecules* **2001**, *34*, 8686.

(2) (a) Feher, F. J.; Newman, D. A.; Walzer, J. F. *J. Am. Chem. Soc.* **1989**, *111*, 1741. (b) Thomas, J. M.; Sankar, G.; Klunduk, M. C.; Attfield, M. P.; Maschmeyer, T.; Johnson, B. F. G.; Bell, R. G. *J. Phys. Chem. B* **1999**, *103*, 8809. (c) Uzunova, E. L.; Nikolov, G. S. *J. Phys. Chem. B* **2000**, *104*, 7299. (d) Kudo, T.; Gordon, M. *J. Phys. Chem. A* **2001**, *105*, 11276. (e) Pescarmona, P. P.; Waal, J. C. v. d.; Maxwell, I. E.; Maschmeyer, T. *Angew. Chem., Int. Ed.* **2001**, *40*, 740. (f) Maxim, N.; Overweg, A.; Kooyman, P. J.; Wolput, J. H. M. C. v.; Hanssen, R. W. J. M.; Santen, R. A. v.; Abbenhuis, H. C. L. *J. Phys. Chem. B* **2002**, *106*, 2203. (g) Murugavel, R.; Davis, P.; Shete, V. S. *Inorg. Chem.* **2003**, *42*, 4696.

(3) (a) Auf der Heyde, T. P. E.; Bürgi, H.-B.; Bürgi, H.; Törnroos, K. W. *Chimica* **1991**, *45*, 38. (b) Törnroos, K. W. *Acta Crystallogr.* **1994**, *C50*, 1646. (c) Frye, C. L.; Collins, W. T. *J. Am. Chem. Soc.* **1970**, *92*, 5586. (d) Bärtsch, M.; Bornhauser, P.; Calzaferri, G.; Imhof, R. *J. Phys. Chem.* **1994**, *98*, 2817. (e) Bornhauser, P.; Calzaferri, G.; Imhof, R. *J. Phys. Chem.* **1996**, *100*, 2035. (f) Muller, R.; Kohne, F.; Sliwinski, S. *J. Prakt. Chem.* **1959**, *9*, 71. (g) Agaskar, P. A. *Inorg. Chem.* **1991**, *30*, 2707.

(4) Sasamori, R.; Okaue, Y.; Isobe, T.; Matsuda, Y. *Science* **1994**, *265*, 1691.

(5) Päch, M.; Stösser, R. *J. Phys. Chem. A* **1997**, *101*, 8360.

(6) Bassindale, A. R.; Pourny, M.; Taylor, P. G.; Hursthouse, M. B.; Light, M. E. *Angew. Chem., Int. Ed.* **2003**, *42*, 3488.

(7) Mattori, M.; Mogi, K.; Sakai, Y.; Isobe, T. *J. Phys. Chem. A* **2000**, *104*, 10868.

(8) (a) Gidden, J.; Shammel, E.; Fee, D. P.; Kemper, P. R.; Anderson, S. E.; Bowers, M. T. *Int. J. Mass Spectrom.* **2003**, *222*, 63. (b) Baker, E. S.; Gidden, J.; Fee, D. P.; Kemper, P. R.; Anderson, S. E.; Bowers, M. T. *Int. J. Mass Spectrom.* **2003**, *227*, 205.

(9) George, A. R.; Catlow, C. R. A. *Chem. Phys. Lett.* **1995**, *247*, 408.

(10) (a) O'Keeffe, M.; Yaghi, O. M. *Chem.−Eur. J.* **1999**, *5*, 2796. (b) Cascales, C.; Gutie'rrez-Puebla, E.; Iglesias, M.; Monge, M. A.; Ruiz-Valero, C. *Angew. Chem., Int. Ed.* **1999**, *38*, 2436. (c) Cascales, C.; Gutie'rrez-Puebla, E.; Iglesias, M.; Monge, M. A.; Ruiz-Valero, C.; Snejko, N. *Chem. Commun.* **2000**, 2145. (d) Conradsson, T.; Dadachov, M. S.; Zou, X. D. *Microporous Mesoporous Mater.* **2000**, *41*, 183. (e) Dadachov, M. S.; Sun, K.; Conradsson, T.; Zou, X. *Angew. Chem., Int. Ed.* **2000**, *39*, 3674. (f) Li, H.; Eddaoudi, M.; Ple'vert, J.; O'Keeffe, M.; Yaghi, O. M. *J. Am. Chem. Soc.* **2000**, *122*, 12409. (g) Li, H.; Eddaouddi, M.; Richardson, D. A.; Yaghi, O. M. *J. Am. Chem. Soc.* **1998**, *120*, 8567.

(11) (a) Villaescusa, L. A.; Lightfoot, P.; Morris, R. E. *Chem. Commun.* **2002**, 2220. (b) Villaescusa, L. A.; Weatley, P. S.; Morris, R. E.; Lightfoot, P. *J. Chem. Soc., Dalton Trans.* **2004**, 820.

(12) Mellouki, A.; Le Bras, G.; Sidebottom, H. *Chem. Rev.* **2003**, *103*, 5077.

(13) Tejerina, B.; Gordon, M. S. *J. Phys. Chem. B* **2002**, *106*, 11764.

(14) Frisch, M. J.; Trucks, G. W.; Schlegel, H. B.; Scuseria, G. E.; Robb, M. A.; Cheeseman, J. R.; Zakrzewski, V. G.; Montgomery, J. A., Jr.; Stratmann, R. E.; Burant, J. C.; Dapprich, S.; Millam, J. M.; Daniels, A. D.; Kudin, K. N.; Strain, M. C.; Farkas, O.; Tomasi, J.; Barone, V.; Cossi, M.; Cammi, R.; Mennucci, B.; Pomelli, C.; Adamo, C.; Clifford, S.; Ochterski, J.; Petersson, G. A.; Ayala, P. Y.; Cui, Q.; Morokuma, K.; Malick, D. K.; Rabuck, A. D.; Raghavachari, K.; Foresman, J. B.; Cioslowski, J.; Ortiz, J. V.; Stefanov, B. B.; Liu, G.; Liashenko, A.; Piskorz, P.; Komaromi, I. R.; Gomperts, R.; Martin, R. L.; Fox, D. J.; Keith, T.; Al-Laham, M. A.; Peng, C. Y.; Nanayakkara, A.; Gonzalez, C.; Challacombe, M.; Gill, P. M. W.; Johnson, B.; Chen, W.; Wong, M. W.; Andres, J. L.; Gonzalez, C.; Head-Gordon, M.; Replogle, E. S.; Pople, J. A. *Gaussian 98*, revision A.11; Gaussian, Inc.: Pittsburgh, PA, 1998.

(15) PQS version 3.1, Parallel Quantum Solutions, 2013 Green Acres Road, Fayetteville, AR 72703.

(16) Becke, A. D. *J. Chem. Phys.* **1993**, *98*, 5648. Lee, C.; Yang, W.; Parr, R. G. *Phys. Rev. B* **1988**, *37*, 785.

(17) (a) Hehre, W. J.; Radom, L.; Pople, J. A.; Schleyer, P. v. R. *Ab Initio Molecular Orbital Theory*; John Wiley & Sons: New York, 1986. (b) Schleyer, P. v. R.; Allinger, N. L.; Clark, T.; Gasteiger, J.; Kollman, P. A.; Schaefer, H. F.,III.; Schreiner, P. R. *The Encyclopedia of Computational Chemistry*; John Wiley & Sons. Ltd.: Chichester, 1998. (c) Foresman, J. B.; Frisch, M. J. *Exploring Chemistry with Electronic Structure Methods*, 2nd ed.; Gaussian, Inc.: Pittsburgh, PA, 1996.

(18) Woon, D. E.; Dunning, T. H. *J. Chem. Phys.* **1993**, *98*, 1358.

(19) (a) Frisch, M. J.; Del Bene, J. E.; Binkley, J. S.; Schaefer, III, H. F. *J. Chem. Phys.* **1986**, *84*, 2279. (b) Schwenke, D. W.; Truhlar, D. G. *J. Chem. Phys.* **1985**, *82*, 2418.

(20) Agaskar, P. A.; Klemperer, W. G. *Inorg. Chim. Acta* **1995**, *229*, 355.

(21) Li, H.; Yaghi, O. M. *J. Am. Chem. Soc.* **1998**, *120*, 10569.

(22) Blukis, U.; Kasai, P. H.; Myers, R. J. *J. Chem. Phys.* **1963**, *38*, 2753.

(23) Siloxane (Si−O, 1.649 Å; ∠SiOSi, 141.7°) and methoxymethane (C−O, 1.413 Å; ∠COC = 112.7°) at B3LYP/6-311++G(2d,p).

(24) Lord, R. C.; Robinson, D. W.; Schumb, W. C. *J. Am. Chem. Soc.* **1957**, *78*, 1327. (b) Almenningen, A.; Bastiansen, O.; Ewing, V.; Hedberg, K.; Tretteberg, M. *Acta Chem. Scand.* **1963**, *17*, 2455. (c) Aronson, J. R.; Lord, R. C.; Robinson, D. W. *J. Chem. Phys.* **1960**, *33*, 1004. (d) Durig, J. R.; Flanagan, M. J.; Kalasinsky, V. F. *J. Chem. Phys.* **1977**, *66* 2775. (e) Koput, J.; Wierzbicki, A. *J. Mol. Spectrosc.* **1983**, *99*, 116. (f) Barrow, M. J.; Ebsworth, E. A.; Harding, M. M. *Acta Crytallogr.* **1979**, *B35*, 2093.

(25) Gokel, G. W.; Trafton, G. E. In *Cation Binding by Macrocycles: Complexation of Cationic Species by Crown Ethers*; Inoue, Y., Gokel, G. W., Eds.; Marcel Dekker: New York, 1990; p 253.

(26) Foster, J. P.; Weinhold, F. *J. Am. Chem. Soc.* **1980** *102*, 7211.

(27) (a) Bassindale, A. R.; Baukov, Y. I.; Borbaruah, M.; Glynn, S. J.; Negrebetsky, V. V.; Parker, D. J.; Taylor, P. G.; Turtle, R. *J. Organomet. Chem.* **2003**, *669*, 154. (b) Loehlin, J. H. *Acta Crystallogr. B* **1993**, *49*, 967. (c) *CRC Handbook of Chemistry and Physics*, 75th ed.; Lide, D. R., Ed.; CRC Press: Boca Raton, FL, 1994.

(28) Fyfe, C. A.; Brouwer, D. H.; Lewis, A. R.; Villaescusa, L. A.; Morris, R. E. *J. Am. Chem. Soc.* **2002**, *124*, 7770.

(29) Huheey, J. E.; Keiter, E. A.; Keiter, R. L. *Inorganic Chemistry: Principles of Structure and Reactivity*, 4th ed.; Harper Collins: New York, 1993.

(30) Moran, D.; Stakl, F.; Jemmis, E. D.; Schaefer, H. F., III; Schleyer, P. v. R. *J. Phys. Chem. A* **2002**, *106*, 5144.

(31) Sun, Q.; Wang, Q.; Yu, J. Z.; Ohno, K.; Kawazoe, Y. J. *Phys.: Condens. Matter* **2001**, *13*, 1931.